

Avoided crossings between bound states of ultracold Cesium dimers

Jeremy M. Hutson

*Department of Chemistry, University of Durham,
South Road, Durham, DH1 3LE, United Kingdom*

Eite Tiesinga and Paul S. Julienne

*Joint Quantum Institute, National Institute of Standards and Technology
and The University of Maryland, Gaithersburg, Maryland 20899-8423, USA*

(Dated: August 21, 2021)

We present an efficient new computational method for calculating the binding energies of the bound states of ultracold alkali-metal dimers in the presence of magnetic fields. The method is based on propagation of coupled differential equations and does not use a basis set for the interatomic distance coordinate. It is much more efficient than the previous method based on a radial basis set and allows many more spin channels to be included. This is particularly important in the vicinity of avoided crossings between bound states. We characterize a number of different avoided crossings in Cs₂ and compare our converged calculations with experimental results. Small but significant discrepancies are observed in both crossing strengths and level positions, especially for levels with l symmetry (rotational angular momentum $L = 8$). The discrepancies should allow the development of improved potential models in the future.

I. INTRODUCTION

Ultracold Cs atoms are of great interest for a number of experiments, which have produced a Bose-Einstein condensate of such atoms [1], formed a cold cloud of Cs₂ dimer molecules [2], probed three-body Efimov physics [3], studied collisional shifts [4] or quantum scattering [5] of atomic clock states, carried out high-resolution molecular spectroscopy [6] or used magnetic fields to switch among a variety of very weakly bound molecular states of the Cs₂ dimer [7, 8]. These experiments all depend upon and take advantage of the collisional interactions between two Cs atoms. Consequently, accurate theoretical and computational models of near-threshold Cs atom scattering and bound states are necessary for maximum understanding of existing experiments and for making quantitative predictions for new experimental domains.

Because of the complex spin structure of two ground-state Cs atoms, many different near-threshold bound states exist and have different magnetic moments. They thus tune differently with magnetic field. When one of these bound states crosses a collision threshold, a low-energy scattering resonance occurs, commonly known as a Feshbach resonance. Extensive study of such resonances has allowed the construction of quite accurate coupled-channel models for calculating the magnetic field-dependent scattering and bound-state properties near collision thresholds [7, 8, 9, 10, 11, 12]. These models incorporate the electron and nuclear spins, their mutual interactions, and the adiabatic Born-Oppenheimer potentials for the $X^1\Sigma_g^+$ and $a^3\Sigma_u^+$ molecular states that correlate with two $^2S_{1/2}$ ground-state Cs atoms. By adjusting the model parameters to fit the measured magnetic fields for resonances in different scattering channels, the model quite accurately predicts near-threshold scattering properties and the binding energies of weakly

bound states within a few GHz of threshold. Such threshold models can also be adapted to treat three-body interactions, for which an accurate knowledge of the threshold two-body bound states is necessary [13]. The models are sensitive to relatively few parameters, and may or may not be adequate when extended into new experimental domains.

Recently, Mark *et al.* [7, 8] have characterized a number of avoided crossings between levels bound by only $E/h \approx 5$ MHz with respect to the energy of two separated Cs atoms in their lowest-energy Zeeman sublevels. Using time-dependent magnetic field ramping, they were able to convert two Cs atoms into a number of different molecular states with different rotational quantum numbers and magnetic moments. Most of the bound states are well described by the existing coupled-channel model in regions far from avoided crossings. However, characterizing the avoided crossings themselves presents problems for the existing computational methods. In particular, Ref. [12] calculated bound states using a method based on a basis set expansion of the radial wavefunctions in a discrete variable representation (DVR). This method can use only a restricted spin basis in determining the molecular bound states because of the large number of grid points required.

The present paper develops an improved computational method that is necessary to calculate and understand the avoided crossings in Cs₂. This method uses a propagator approach [14] in place of a radial basis set to represent the molecular bound states. It can readily be adapted to threshold states of other molecules [15, 16]. The propagator approach is computationally much cheaper than the DVR approach and as a result can include many more coupled spin channels. The new approach is used to compare the calculated and observed properties of the avoided crossings, in order to identify aspects of the ground-state coupled-channel

model for Cs₂ that are still in need of improvement.

II. COMPUTATIONAL METHODS

The present work solves the bound-state Schrödinger equation for Cs₂ using two independent methods. In either case the Hamiltonian may be written

$$\frac{\hbar^2}{2\mu} \left[-R^{-1} \frac{d}{dR^2} R + \frac{\hat{L}^2}{R^2} \right] + \hat{h}_1 + \hat{h}_2 + \hat{V}(R), \quad (1)$$

where μ is the reduced mass and \hat{L}^2 is the operator for the end-over-end angular momentum of the two atoms about one another. The monomer Hamiltonians including Zeeman terms are

$$\hat{h}_j = \zeta \hat{i}_j \cdot \hat{s}_j + g_e \mu_B B \hat{s}_{zj} + g_n \mu_B B \hat{i}_{zj}, \quad (2)$$

where \hat{s}_1 and \hat{s}_2 represent the electron spins of the two atoms and \hat{i}_1 and \hat{i}_2 represent nuclear spins. g_e and g_n are the electron and nuclear g -factors, μ_B is the Bohr magneton, and \hat{s}_z and \hat{i}_z represent the z -components of \hat{s} and \hat{i} along a space-fixed Z axis whose direction is defined by the external magnetic field B . The interaction between the two atoms $\hat{V}(R)$ is given by Stoof *et al.* [17] as the sum of two terms,

$$\hat{V}(R) = \hat{V}^c(R) + \hat{V}^d(R). \quad (3)$$

Here $\hat{V}^c(R) = V_0(R)\hat{P}^{(0)} + V_1(R)\hat{P}^{(1)}$ is an isotropic potential operator that depends on the potential energy curves $V_0(R)$ and $V_1(R)$ for the respective $X^1\Sigma_g^+$ singlet and $a^3\Sigma_u^+$ triplet states of the diatomic molecule. The singlet and triplet projectors $\hat{P}^{(0)}$ and $\hat{P}^{(1)}$ project onto subspaces with total electron spin quantum numbers 0 and 1 respectively. Figure 1 shows the two potential energy curves for Cs₂. The $\hat{V}^d(R)$ term represents small, anisotropic spin-dependent couplings that are responsible for the avoided crossings discussed in this paper and are discussed further in Section III below.

The first method for finding eigenvalues is a conventional full matrix diagonalization in a discrete variable representation (DVR) [18]. It uses a basis set made up of products of internal and radial functions. The internal Bose-symmetrized basis set is made up of functions in which the operators \hat{L}^2 and \hat{h}_j are diagonal, that is,

$$|\alpha_1 m_{f1}\rangle |\alpha_2 m_{f2}\rangle |LM_L\rangle, \quad (4)$$

where $|LM_L\rangle$ and $|\alpha_j m_{fj}\rangle$ respectively represent the eigenstates of \hat{L}^2 and the B -dependent monomer Hamiltonian \hat{h}_j , and where M_L and m_{fj} are projection quantum numbers along the magnetic field direction. When $B = 0$, $|\alpha_j m_{fj}\rangle = |(s_j i_j) f_j m_{fj}\rangle$, where f_j is the total spin of atom j and m_{fj} is its space-fixed projection. As B increases from zero, different f_j values become mixed.

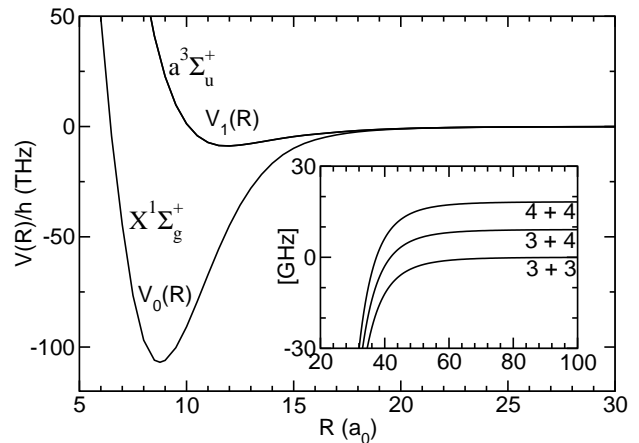


FIG. 1: Molecular potential energy curves $V_0(R)$ and $V_1(R)$ for the respective singlet and triplet states of Cs₂ correlating with two separated $^2S_{1/2}$ ground-state atoms. The inset shows an expanded view of the long-range potentials separating to the two different $f = 3$ and 4 hyperfine states of the $^2S_{1/2}$ atom with nuclear spin $i=7/2$ and magnetic field $B = 0$. The inset shows the adiabatic potentials obtained from diagonalizing the matrix form of the operator $\hat{h}_1 + \hat{h}_2 + \hat{V}(R)$ at each R for the case of $L = 0$, $M_F = +6$. There are 5 channels, and the 3 + 4 and 4 + 4 separated-atom limits are doubly degenerate at $B = 0$. All 5 channels have the same long-range variation as $-C_6/R^6$, with $C_6 = 6860 E_h a_0^6$ [12] ($E_h = 4.3597 \times 10^{-18}$ J is the Hartree and $a_0 = 0.0529177$ nm is the Bohr radius). The level crossings discussed in this paper are for very weakly bound levels that lie within about $E/h \approx 5$ MHz of the dissociation limit to two $\{f m_f\} = \{3, +3\}$ atoms in the magnetic field range from 0 mT to 5 mT.

The DVR radial functions are unevenly spaced collocation points obtained from a nonlinear coordinate transformation [19].

This DVR method requires diagonalizing a large $N \times N$ matrix, the dimension of which is given by the product of the number of spatial collocation points N_c and the number of spin basis functions N_s . We use the LAPACK subroutine DSPEVX to find a selected range of eigenvalues and eigenvectors [20]. In order to use a direct diagonalization procedure to calculate the bound-state energies [21] shown in Refs. [8, 12], the magnitude of $N = N_c N_s$ was limited to around 25000 using a processor with 4 GB of memory. With $N_c \approx 800$, in order to give 5 points per node with about 150 nodes for threshold wave functions, the number of spin basis functions is thus restricted to be about $N_s \approx 35$. When this is fewer than is needed for a complete calculation, an approximation scheme becomes necessary, as described in Section III.

The second method avoids the use of a basis set for the interatomic distance R and instead relies on propagation of coupled differential equations [14]. In this case the Bose symmetrized basis set used is a fully decoupled set,

$$\Phi_k = |s_1 m_{s1}\rangle |i_1 m_{i1}\rangle |s_2 m_{s2}\rangle |i_2 m_{i2}\rangle |LM_L\rangle. \quad (5)$$

The compound channel index k is used to simplify nota-

tion and implies values of all the quantum numbers in the basis set. While the choice of the basis sets in Eqs. (4) and (5) represent different approaches, they are equivalent for representing molecular energy levels when the two basis sets span the same space. There is a simple unitary transformation between the two basis sets. The matrix elements of the different terms in the Hamiltonian in basis set (5) are given in the Appendix.

In the propagation method, we expand the total wavefunction for state n as

$$\Psi_n = R^{-1} \sum_k \Phi_k \psi_{kn}(R). \quad (6)$$

Substituting into the Schrödinger equation and projecting onto each channel function in turn gives a set of coupled equations for the radial channel functions $\psi_{kn}(R)$,

$$\frac{d^2 \psi_{jn}}{dR^2} = \sum_k [W_{jk}(R) - \varepsilon \delta_{jk}] \psi_{kn}(R), \quad (7)$$

where δ_{jk} is the Kronecker delta, ε is the energy E scaled by $2\mu/\hbar^2$, and

$$W_{jk}(R) = \int \Phi_j^* \left[\frac{\hat{L}^2}{R^2} + \frac{2\mu}{\hbar^2} (\hat{h}_1 + \hat{h}_2 + \hat{V}(R)) \right] \Phi_k d\tau, \quad (8)$$

where $d\tau$ indicates integration over all coordinates except R . If there are N_s basis functions, the required solution $\psi_n(R)$ is a column vector of order N_s with elements $\psi_{kn}(R)$. However, Eq. 7 has N_s independent solution vectors at any energy, so that until the boundary conditions are applied $\psi_n(R)$ is an $N_s \times N_s$ wavefunction *matrix*.

The Schrödinger equation can be solved to find an $N_s \times N_s$ wavefunction matrix at any energy E . In practice it is numerically stabler to propagate the log-derivative matrix $Y(R) = [d\psi_n/dR][\psi_n(R)]^{-1}$. However, a solution that satisfies bound-state boundary conditions can be found only at the eigenvalues E_n . Solutions are propagated outwards from a point R_{\min} in the inner classically forbidden region and inwards from a point R_{\max} at long range to a matching point R_{mid} . The outwards and inwards solutions are designated $Y^+(R)$ and $Y^-(R)$. If E is an eigenvalue of the coupled equations, there must exist a wavefunction vector $\psi_n(R_{\text{mid}}) = \psi_n^+(R_{\text{mid}}) = \psi_n^-(R_{\text{mid}})$ for which the derivatives also match,

$$\left. \frac{d\psi_n^+}{dR} \right|_{R_{\text{mid}}} = \left. \frac{d\psi_n^-}{dR} \right|_{R_{\text{mid}}}, \quad (9)$$

so that

$$Y^+(R_{\text{mid}})\psi_n(R_{\text{mid}}) = Y^-(R_{\text{mid}})\psi_n(R_{\text{mid}}). \quad (10)$$

Thus $\psi_n(R_{\text{mid}})$ is an eigenvector of $Y^+(R_{\text{mid}}) - Y^-(R_{\text{mid}})$ with eigenvalue 0. It is thus possible to locate eigenvalues of the Schrödinger equation by propagating solutions of the coupled equations and searching for zeroes in the eigenvalues of the log-derivative matching matrix

$Y^+(R_{\text{mid}}) - Y^-(R_{\text{mid}})$ as a function of energy. This approach is much stabler for large multichannel problems than the older approach [22] of searching for zeroes of the *determinant* of the matching matrix.

The major advantage of the propagator method is that the matrices handled are only of dimension $N_s \times N_s$, where N_s is the number of *internal* basis functions. The computational cost is proportional to N_s^3 but only *linear* in the number of propagation steps. By contrast, a full diagonalization with N_c radial basis functions (collocation points) involves matrices of dimension $N_s N_c \times N_s N_c$. The computational cost is proportional to $N_s^3 N_c^3$. Since N_c typically needs to be greater than 500 for the present application, the propagator approach is much cheaper.

The BOUND program [23] is a general-purpose package to solve the bound-state Schrödinger equation using propagator methods. The algorithms used are described in more detail in Ref. 14. For the purpose of the present work we have generalised the BOUND package in three significant respects:

1. We have generalised the structure of the code so that it can handle coupled equations in basis sets that are not diagonal at $R = \infty$;
2. We have implemented the specific set of coupled equations required for Cs_2 with the basis set of Eq. 5;
3. We have added an option to use the log-derivative propagator of Alexander and Manolopoulos [24], which is based on Airy functions and allows very large step sizes at long range.

In the presence of a magnetic field, the only rigorously conserved quantum numbers are $M_{\text{tot}} = m_{f1} + m_{f2} + M_L = m_{s1} + m_{s2} + m_{i1} + m_{i2} + M_L$ and the total parity $(-1)^L$. This leads to an infinite number of channels. However, L and $M_F = m_{f1} + m_{f2}$ are very good approximate quantum numbers because the only term in the Hamiltonian that is off-diagonal in them is the small anisotropic coupling term \hat{V}^d . In either computational approach it is possible to restrict the number of channels by selecting only one or a few values of L and all or a subset of possible M_F values. Here we consider the case studied experimentally by Mark *et al.* [8], who used Cs atoms in their lowest energy hyperfine state with $m_f = +3$ to make Cs_2 molecules with $M_{\text{tot}} = +6$. The number of channels with $L = 0, 2, 4, 6, 8$, including all allowed M_F values, are 5, 23, 46, 76, 103, respectively. Thus, for example, a full calculation including all channels with $L = 4, 6$ and 8 requires 225 channels.

In practical terms, for example, a run with the DVR method to find 28 bound states within 3 GHz of the $E = 0$ threshold for Cs_2 for a single magnetic field with 30 channels and 720 collocation points took about 7 hours on a 2.4 GHz processor. With the propagator approach we were able to find selected near-dissociation levels for 30 channels in about 40 seconds per level with a 2.0 GHz

processor. The great advantage of the propagator approach was demonstrated by our ability to find levels with 225 channels in about 45 minutes per level. A calculation with 225 channels would not be possible at all using the DVR method with a direct eigenvalue solver.

III. COMPARISON OF COMPUTATIONAL RESULTS

The DVR and propagator calculations described here both use the same potential model, with the parameters given by Chin *et al.* [12]. The potential energy curves are based on the *ab initio* calculations of Krauss and Stevens [25]. The singlet and triplet scattering lengths a_S and a_T , the long-range coefficients C_6 and C_8 , and a scaling factor S_C for the second-order spin-orbit coupling were adjusted by Chin *et al.* to reproduce a substantial number of Feshbach resonances with $L \leq 4$.

Figure 2 shows an example of weakly bound levels of the Cs_2 molecule with $M_{\text{tot}} = +6$ in the 0 mT to 6 mT range of B . Many of these levels have been probed in the experiment of Mark *et al.* [8]. The figure also shows the bound-state classification scheme of Chin *et al.* [12], namely $FL(M_F)$, where F is the resultant of the separated-atom spins f_1 and f_2 and M_F is its projection defined above. Like f_1 and f_2 , F is a good approximate quantum number for labeling near-threshold levels at low B . Quantum numbers $L = 0, 2, 4, 6, 8$ are represented by labels s, d, g, i, l , respectively. M_L need not be specified since $M_L = M_{\text{tot}} - M_F$. Fig. 2 shows levels with $L \leq 4$ obtained from a DVR calculation that included only basis functions for a single L and M_F . This neglects the small off-diagonal couplings between levels with different L and M_F quantum numbers due to \hat{V}^d , so that levels of different symmetry show crossings rather than avoided crossings in Fig. 2.

For ground-state alkali-metal atom interactions, the \hat{V}^d operator has the form of spin-dipolar coupling

$$\hat{V}^d(R) = \lambda(R) (\hat{s}_1 \cdot \hat{s}_2 - 3(\hat{s}_1 \cdot \vec{e}_R)(\hat{s}_2 \cdot \vec{e}_R)), \quad (11)$$

where \vec{e}_R is a unit vector along the internuclear axis and λ is an R -dependent coupling constant, which for our model is

$$\lambda(R) = E_h \alpha^2 \left(\frac{1}{(R/a_0)^3} - 0.071968 e^{-0.83[(R/a_0)-10]} \right), \quad (12)$$

where $\alpha \approx 1/137$ is the fine structure constant. At large R the coupling becomes the long-range dipolar interaction between the spins on the separated atoms that varies as $1/R^3$ [17, 26]. In the short-range region of chemical bonding the magnitude of $\lambda(R)$ is primarily determined by the second-order spin-orbit coupling term represented by the exponential term [12, 27, 28, 29].

The crossings in Fig. 2 become avoided crossings when the small interactions due to \hat{V}^d are taken into account. The energy splitting at the crossing varies greatly, depending on the quantum numbers of the two levels. In

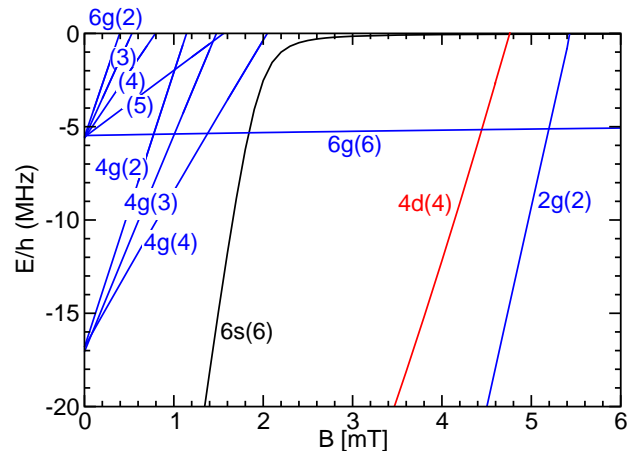


FIG. 2: Bound state energy E/h as a function of B for levels of the Cs_2 molecules with even $L \leq 4$ and $M_{\text{tot}} = +6$. Energies are given relative to the energy of two Cs atoms in their ground Zeeman sublevel ($f = 3$, $m_f = +3$). The $FL(M_F)$ labeling scheme is shown for each level. Off-diagonal coupling between levels with different $FL(M_L)$ quantum numbers is neglected in this calculation.

first order, the \hat{V}^d operator couples states $FL(M_F)$ and $F'L'(M'_F)$ according to the selection rules $|L - L'| = 0$ or 2 , $|F - F'| = 0, 1, \text{ or } 2$, and $|M_F - M'_F| = 0, 1, \text{ or } 2$. These selection rules immediately follow from the tensor form of the operator in Eq. (11), as given by Stoof *et al.* [17], who write Eq. (11) as a sum of products of $L = 2$ spherical harmonic components $Y_{LM_L}(\vec{e}_R)$ and rank 2 spin tensor components. We refer to a crossing as direct when there is a first order coupling of the two states involved and indirect when there is not.

The success of a calculation of the Cs_2 energy levels and their avoided crossings depends on the sufficiency of the basis set expansion of the wave function. Suppose we wish to calculate the energy of one $FL(M_F)$ state that crosses a different $F'L'(M'_F)$ state. It is necessary to include sufficient basis functions to represent each state adequately, and to represent their interaction. This is simplified by taking advantage of the selection rules described above. In order to represent a level with a given $FL(M_F)$, it is necessary to include all basis functions with the same set of three quantum numbers, since such levels are coupled by terms due to the strong central potential \hat{V}^c . A level calculated with such a basis is coupled through the \hat{V}^d operator to other levels in which one or more of the three quantum numbers are different. Such off-diagonal coupling causes shifts in level positions and also induces avoided crossings.

In the propagator calculations, the basis set usually includes all functions with L and L' of the levels in question consistent with M_{tot} . Additional basis functions with different quantum numbers L_i are added to account for shifts and crossings due to coupling of L or L' with L_i . The propagator basis is specified by giving L , L' , and a list of additional values L_i needed to account for higher-

order coupling. In the DVR calculations, the basis sets are additionally limited by restricting the calculation to functions with $L(M_F)$, $L'(M'_F)$ and additional quantum numbers $L_i(M_{F,i})$ as needed. Thus the basis set is specified by giving the list $L(M_F)L'(M'_F)[L_i(M_{F,i})]$. Some propagator calculations were done with a similarly restricted list to verify that the two methods gave exactly equivalent results. Neither the propagator nor DVR cal-

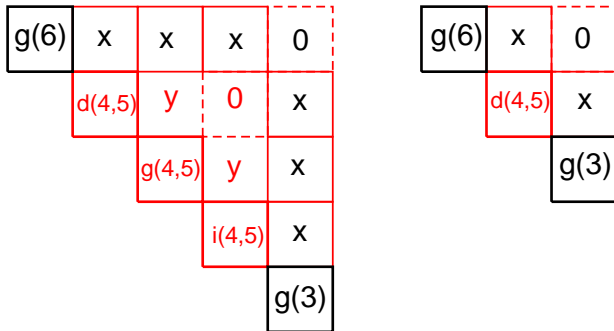


FIG. 3: Example of coupling between different $L(M_F)$ symmetry blocks with the symmetry of the dipole-dipole interaction of \hat{V}^d . Each block represents a Hamiltonian matrix for spin states with the $L(M_F)$ values indicated. The labels “x” and “y” indicate the existence of nonvanishing coupling due to \hat{V}^d ; a “0” indicates no coupling. The case shown is for a $g(6)$ and a $g(3)$ level, which have no direct coupling. The left panel shows the symmetries that give rise to second-order interactions between the two levels and thus contribute to the strength of the avoided crossing between them. The right panel shows a truncated set of interactions through intermediate $d(4)$ and $d(5)$ levels.

Figure 3 illustrates the size of the basis set needed, as governed by the selection rules on \hat{V}^d coupling. Since the matrix elements of \hat{V}^d are relatively small, they are normally of practical significance only through second order. Thus it is necessary to include only intermediate levels with L_i and $M_{F,i}$ that differ from L or L' and M_F or M'_F by at most 2 units. Any higher-order couplings would be much smaller than those discussed here. Thus, in order to represent the crossing of a $6g(6)$ and a $4g(3)$ level, for which there is no first-order direct coupling, d -, g -, or i -basis functions with $M_F = 4$ and 5 need to be included in the basis, as shown in Fig. 3. To represent additional second-order shifts of the two g levels, d -, g - and i -basis functions with $M_F = 1, 2, 7$ and 8 also need to be added.

Figure 4 illustrates calculations with different basis sets, comparing energies calculated with the propagator and DVR methods for the crossing of the $4g(3)$ and $6g(6)$ levels near 1.0 mT. Table I tabulates the positions and strengths of this crossing, as well as a number of others. The position B_0 of the crossing is defined as the field at which the two levels are closest together and the strength $2V$ is the minimum of the difference between

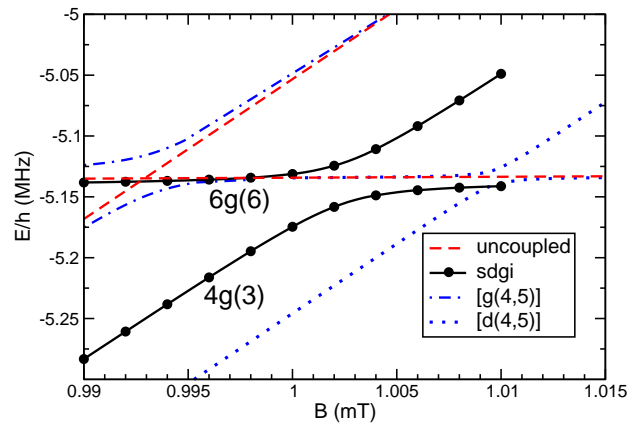


FIG. 4: Calculated energy levels E/h with $M_{tot} = +6$ as a function of magnetic field B near the crossing of the $4g(3)$ level with the $6g(6)$ level near 1.0 mT. The points and solid line show the propagator calculation with a $sdgi$ basis set. The dashed lines show the crossing levels from two uncoupled DVR calculations with $g(3)$ or $g(6)$ basis functions only. The dash-dot and dotted lines show the crossing levels from DVR calculations with added $g(4, 5)$ and $d(4, 5)$ functions respectively. The DVR calculation with $i(4, 5)$ basis functions is not shown, but lies near the uncoupled crossing and has a very small splitting, indicating very weak second-order coupling through distant i states.

the two energies as a function of B ; $2V$ is used since the splitting is twice the effective coupling matrix element V in a 2-level representation of the crossing [8]. We have verified that the two methods give identical results within numerical accuracy when exactly equivalent basis sets are used. Since there is no direct interaction between the two crossing levels in this case, the splitting at the crossing originates principally in second-order interactions mediated through distant levels of d , g , or i symmetry with $M_F = 4$ or 5. However, as mentioned above, second-order couplings to levels with other M_F values can cause additional shifts. Both bound and scattering states can contribute, and the contribution from any given distant state varies inversely with its separation in energy from the crossing. Intermediate g levels are the closest in energy to the crossing, whereas intermediate i levels are the most distant. In Figure 4, the $sdgi$ basis set used in the propagator calculation is effectively complete. It may be seen that a calculation including only the $g(4, 5)$ intermediate states captures most of the crossing strength but does not reproduce the level shifts well. Conversely, a calculation including only the $d(4, 5)$ states gives a crossing strength that is much too small but overestimates the level shifts. The contributions to the crossing strength from different intermediate states are far from additive. There are no experimental results for this crossing.

Figure 5 illustrates a different case, a $4g(4) - 6g(6)$ crossing with a splitting that is about 8 times larger at the crossing. This is a case where the two states involved have a direct coupling to one another through

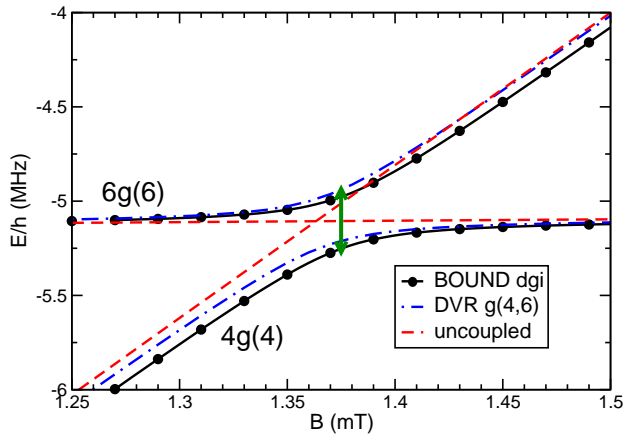


FIG. 5: Calculated energy levels E/h with $M_{\text{tot}} = +6$ as a function of magnetic field B near the crossing of the $4g(4)$ level with the $6g(6)$ level near 1.0 mT. The points and solid line show the propagator calculation with a dgi basis set. The dashed lines show the crossing levels from two uncoupled DVR calculations with $g(4)$ or $g(6)$ basis functions only. The dash-dot lines show the avoided crossing from a DVR calculation with only the direct coupling in the $g(4,6)$ basis set included. The doubled-headed arrow at the position of the propagator crossing shows the measured splitting [8]. The actual experimental crossing was observed 0.046 mT lower in B value than the propagator crossing.

\hat{V}^d . While additional second-order coupling can change the position and strength of the crossing slightly, the direct coupling is dominant and the restricted-basis DVR calculation agrees much better with the full propagator calculations. Both are in reasonable agreement with the measured splitting of the crossing [8]. However, the calculated position in B needs to be shifted by -0.046 mT to agree with the measured position [8]. This remaining discrepancy reflects a real deficiency in the parameters of our potential model as discussed below.

Figure 6 shows the difference between the upper and lower branches of the crossing for the case of the $4d(4) - 6g(6)$ crossing near 4.5 mT. This is another case of direct coupling, where the measured and calculated crossings agree well in coupling strength, although the calculated position needs to be shifted by $+0.034$ mT to agree with the measured one.

Table I show comparisons between the propagator and DVR calculations for a number of other crossings in Figure 2. Crossing positions generally agree within about 0.01 mT among the different basis sets. Relatively good agreement between propagator and DVR coupling strengths $2V$ is seen in the cases where there is direct coupling between the two crossing levels, or where the DVR method includes all second-order intermediate states allowed by the symmetry of the \hat{V}^d operator. However, for higher- L crossings it was usually necessary to select a subset of the allowed intermediate states to make DVR calculations feasible. In such cases the DVR method can give unreliable results, depending on the choice of re-

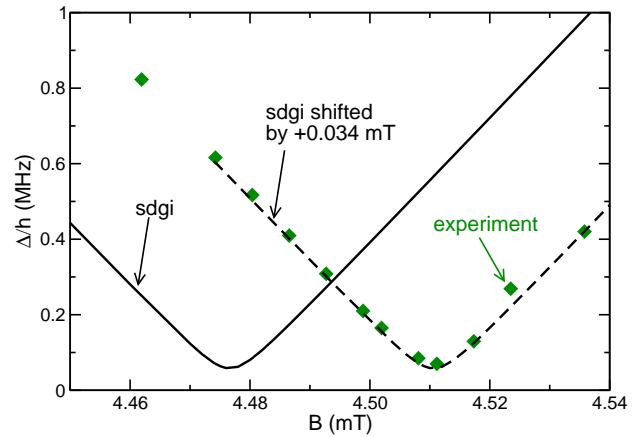


FIG. 6: Calculated energy difference Δ/h between the $6g(6)$ and $4d(4)$ levels with $M_{\text{tot}} = +6$ as a function of magnetic field B . The solid line is from a propagator calculation with the $sdgi$ basis. The diamonds show the experimental results obtained by Ferlaino *et al.* using their more accurate field modulation method [30]. The dashed line shows the calculated points shifted by $+0.034$ mT. The DVR calculation (not shown) with direct coupling included in the $d(4)g(6)$ basis is virtually identical to the dashed line when the DVR results are shifted by $+0.062$ mT.

stricted basis set.

Figure 7 shows calculated bound states for s and d levels on a broader energy scale. (Levels with other symmetries are not shown). A DVR calculation with a full sd basis is possible in this case. The $6s(6)$ and $4d(4)$ uncoupled levels show two crossings. The low-field crossing around 0.24 mT occurs near the observed location (0.72 mT) of a three-body Borromean state of the Cs_3 trimer associated with the exotic Efimov physics of this species [3]. Lee *et al.* [13] used the last two $6s(6)$ two-body states of the Cs_2 dimer to construct the parameters for full three-body calculations of bound states and recombination coefficients in the 0 mT to 3 mT range. While their method was able to give semi-quantitative agreement with the measurements, the avoided crossing of the $6s(6)$ level with the $4d(4)$ level needs to be taken into account in subsequent calculations because of the mixed spin character of the target molecular state produced by the three-body recombination in this region of B . The strong $s - d$ interactions modify the s -wave scattering length at small B , but this is easy to take into account by including s and d basis functions in scattering calculations.

The higher-field $6s(6) - 4d(4)$ crossing near 4.8 mT has been studied in Refs. [8, 31]. Figure 9 shows an expanded view of the very-near-threshold region of this crossing and the additional $6s(6) - 2g(2)$ crossing near 5.4 mT. The interaction between s and d states results in an overall shift in the binding energy of the $6s(6)$ level, where the uncoupled level is too high in energy. This case illustrates one advantage of the propagator method over the DVR method. The latter has to use a finite range of

spatial points and is restricted by the length of the “box” in which the calculation is carried out. When this length is too large, the number of the spatial collocation points can become too large for practical calculations. A 5000 a_0 “box” is sufficient for levels with binding energies on the order of 40 kHz, since the scattering length, which gives an indication of the “size” of the weakly bound molecular levels [15], is on the order of 1000 $a_0 \ll 5000 a_0$. Such restrictions on spatial grid do not apply to the propagator method, which is capable of calculating levels arbitrarily close to $E = 0$, as long as the propagation is to sufficiently large distances. Since the propagator used can take very large steps at long range, this presents no

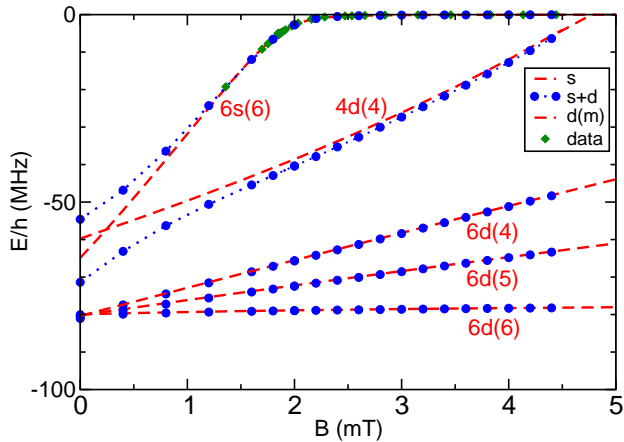


FIG. 7: Energy levels E/h as a function of B for the Cs_2 molecule for $L = 0$ and 2 only with $M_{\text{tot}} = +6$ (g and l levels are not shown). The dashed lines show the DVR levels calculated with the uncoupled $s(6)$ and $d(M_F)$ basis sets, where $M_F = 4, 5, \text{ or } 6$. The diamonds show the results of Mark *et al.* [8]. The $4d(4)$ level crosses the $6s(6)$ level twice, near 0.24 mT and 4.77 mT. The closed circles and dotted lines show the levels obtained from a DVR calculation with an sd basis. A propagator calculation with a full sdg basis shows negligible differences for this case.

IV. COMPARISON WITH EXPERIMENT

When the basis set is sufficiently large, there is good overall agreement between our calculations and the experimental measurements, as already noted in relation to Figs. 5 and 6. Table II lists other examples, including the crossings of the $6g(6)$ level with the $6l(M_F)$ levels shown in Fig. 8. Since the potentials and second-order spin-orbit coupling of the model were originally adjusted to reproduce Feshbach resonances due to zero-energy bound states of d and g symmetry, the positions of crossings between s , d , and g levels tend to be accurate to within the model uncertainties, which are on the order of 0.05 mT or less [10, 12]. On the other hand, the levels of l symmetry, corresponding to $L = 8$, are off by up to 0.5 mT, a much larger amount. One plausible reason for this has to

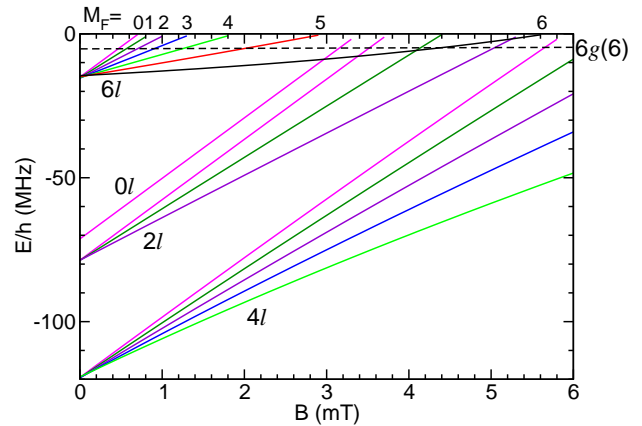


FIG. 8: Energy levels E/h as a function of B for the Cs_2 molecule for $L = 8$ only with $M_{\text{tot}} = +6$. The solid lines show the DVR levels calculated with the uncoupled $l(M_F)$ basis sets, where $M_F = 0, \dots, 6$. The dashed line shows the $6g(6)$ level for which avoided crossings have been calculated

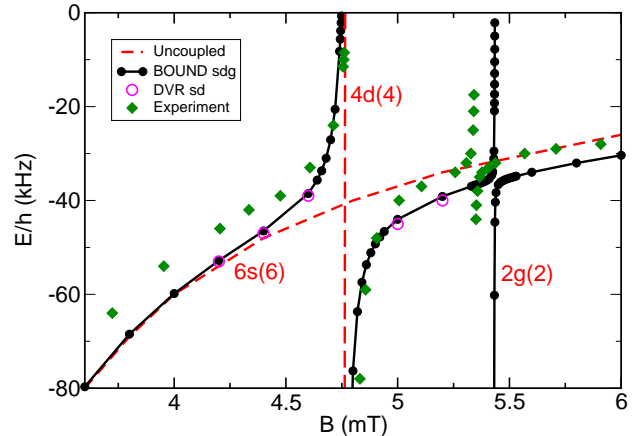


FIG. 9: Expanded view of the crossing in Fig. 7 of the $4d(4)$ and $6s(6)$ levels near 4.8 mT. The long dashed line shows the uncoupled calculation with the $s(6)$ and $d(4)$ basis sets. The solid lines show the propagator calculations with an sdg basis. The upper crossing near 5.4 mT is due to a $2g(2)$ level. The open circles show DVR calculations with a full sd basis in a finite box of 5000 a_0 . The diamonds show experimental results of Lange *et al.* [32].

do with the large rotational energy of the $6l(M_F)$ levels that cross the $6g(6)$ level. The $6g(6)$ level has the vibrational character of the second $6s(6)$ vibrational level below the lowest separated-atom limit, with about 110 MHz of $l = 4$ rotational energy added. The crossing $6l(M_F)$ levels, by contrast, have the vibrational character of the third vibrational level below the limit, with about 740 MHz of rotational energy added to bring them near threshold. More deeply bound levels with more rotational energy can have larger errors due to deficiencies in the model potentials. An error of only a few parts per 1000 in the rotational energy can lead to a 0.5 mT error

TABLE I: Levels crossing the $6g(6)$ level of the Cs_2 molecule with a binding energy near -5 MHz relative to the energy of two atoms in their lowest energy hyperfine state at each B . The columns label the symmetry of the crossing state, the computational method (propagator or DVR), the L functions in the basis set used for the calculation (only intermediate basis states are listed for the DVR method, since basis states for the two crossing states are automatically included), and the position B_0 , energy E/h , and splitting $2V/h$ of each crossing.

| State | Method | Basis | B_0 [mT] | E/h [MHz] | $2V/h$ [kHz] |
|-------|------------|--------------------|---------------|----------------|-----------------|
| 4g(2) | propagator | g | 0.7615 | -5.180 | 3.6 |
| | propagator | dg | 0.7670 | -5.192 | 1.0 |
| | propagator | $sdgi$ | 0.7617 | -5.152 | 1.5 |
| | DVR | $g(2,6)[d(4)]$ | 0.7745 | -5.152 | 2.3 |
| 6l(3) | propagator | gil | 0.9181 | -5.135 | 21.2 |
| | DVR | $g(6)l(3)[i(4,5)]$ | 0.9112 | -5.138 | 21.7 |
| 4g(3) | propagator | sdg | 1.0105 | -5.169 | 37.3 |
| | propagator | $sdgi$ | 1.0024 | -5.138 | 33.5 |
| | DVR | $g(3,6)[d(4,5)]$ | 1.0097 | -5.134 | 12.1 |
| | DVR | $g(3,6)[g(4,5)]$ | 0.9935 | -5.134 | 32.9 |
| | DVR | $g(3,6)[i(4,5)]$ | 0.9937 | -5.1314 | 1.1 |
| 6l(4) | propagator | gil | 1.2715 | -5.088 | 43.6 |
| 4g(4) | propagator | g | 1.368 | -5.14 | 264. |
| | propagator | dgi | 1.375 | -5.11 | 277. |
| | DVR | $g(4,6)$ | 1.367 | -5.10 | 265. |
| 6s(6) | propagator | sdg | 1.8648 | -5.114 | 44.8 |
| | propagator | $sdgi$ | 1.8664 | -5.079 | 44.8 |
| 6l(5) | propagator | gil | 2.0089 | -5.056 | 66.6 |
| 6l(6) | propagator | gil | 4.3211 | -4.890 | 77.6 |
| 4d(4) | propagator | dg | 4.4403 | -4.937 | 55.5 |
| | propagator | $sdgi$ | 4.4766 | -4.885 | 57.6 |
| | DVR | $d(4)g(6)$ | 4.4485 | -4.905 | 53.0 |
| 2g(2) | propagator | g | 5.1906 | -4.887 | < 0.1 |
| | propagator | dgi | 5.1176 | -4.842 | 9.5 |

in the crossing positions for $6l(M_F)$ levels.

Additional information is contained in the coupling strengths that govern the closest approach $2V$ between levels at avoided crossings. In the calculations, this quantity is determined largely by the second-order spin-orbit contribution to \hat{V}^d . This is a relatively poorly determined parameter in our model and is uncertain to about 15% [10].

Several different experimental methods have been used to determine coupling strengths. Mark *et al.* [7] used a method based on Stückelberg interferometry, which gives precise measurements of the energy difference between the two states. Mark *et al.* [8] used a different method based on integrating magnetic moment values. This gives absolute energies for the two states (rather than just the difference between them) but is now believed to overestimate the coupling strengths in some cases [33], especially

for crossings between states with very different magnetic moments. Some crossing strengths were also estimated from a Landau-Zener approach. Lastly, Ferlaino *et al.* [30] have used a method in which transitions are induced by modulating the magnetic field [34]. This is the most precise of the different methods.

TABLE II: Comparison of results from the best propagator calculation with the experimental results for selected level crossings with the $6g(6)$ state. The columns label the symmetry of the crossing state, the origin of the value, the L functions in the basis set used for the calculation, and the position B_0 , energy E/h , and the energy splitting $2V/h$ for each crossing. The lines labeled “Exp” show the experimental values.

| State | method | basis | B_0 [mT] | E/h [MHz] | $2V/h$ [kHz] |
|-------|------------------|--------|------------|-------------|--------------|
| 6l(3) | propagator | gil | 0.9181 | -5.135 | 21.2 |
| | Exp ^a | | 1.122(2) | | 32(6) |
| | Exp ^b | | 1.1339(1) | | 28(2) |
| 6l(4) | propagator | gil | 1.2715 | -5.088 | 43.6 |
| | Exp ^a | | 1.550(3) | | 128(26) |
| 4g(4) | propagator | dgi | 1.375 | -5.11 | 277. |
| | Exp ^a | | 1.329(4) | | 328(60) |
| | Exp ^c | | 1.357(1) | | 291.4(8) |
| 6s(6) | propagator | $sdgi$ | 1.8664 | -5.079 | 44.8 |
| | Exp ^c | | 1.8651(3) | | 58(17) |
| 6l(5) | propagator | gil | 2.0089 | -5.056 | 66.6 |
| | Exp ^a | | 2.53(1) | | 126(44) |
| 4d(4) | propagator | $sdgi$ | 4.4766 | -4.885 | 57.6 |
| | Exp ^a | | 4.515(4) | | 240(42) |
| | Exp ^c | | 4.5106(3) | | 78(9) |

a. Reference [8]
b. Reference [7]
c. Reference [30].

The crossing strengths for various different levels crossing the $6g(6)$ level near 5 MHz are compared with the available experimental values in Table II. The most reliable experimental results are those from Stückelberg oscillations [7] and magnetic field modulation [33] for the $6l(3)$, $4g(4)$, $6s(6)$ and $4d(4)$ levels. The $6l(3)$ and $6s(6)$ levels are indirectly coupled to $6g(6)$, and for both these the calculated crossing strength is about 25% lower than the best experimental value. The $4g(4)$ and $4d(4)$ levels are directly coupled to $6g(6)$; for the $4g(4)$ level the calculated crossing strength is about 5% lower than experiment, while for the $6s(6)$ level the discrepancy is larger but is within the experimental error bars. This suggests that the strength of the coupling term $V^d(R)$ is underestimated but within the error range of Leo *et al.* [10].

Some of the other crossings in Table II show larger differences between experiment and theory, but in all these cases the experimental value was obtained using the less reliable magnetic moment method. The possible experimental errors for the magnetic moment approach are illustrated by the $4d(4)$ crossing, where it gives a cross-

ing strength a factor of 3 larger than the more accurate magnetic field modulation method. It would be very interesting to remeasure the $6l(4)$, $6l(5)$ and other crossings in order to establish whether there is a consistent relative error between experiment and theory.

Errors in the level positions can result from deficiencies in either the long-range or the short-range part of the model potentials. As discussed above, there are remaining discrepancies in level positions of up to 0.05 mT for s , d , and g levels, and up to 0.5 mT for l levels. Further improvements in the potential model are thus needed for this important prototype system. This is particularly important for predicting the resonances and crossings in the 80 mT region, where interesting Efimov physics is predicted [13] and even greater sensitivity to model errors is expected. A major advantage of the propagator method introduced here is that it is inexpensive enough to be used to determine model parameters by least-squares fitting to level energies and locations and strengths of level crossings.

V. CONCLUSIONS

We have presented a new computational method for calculating bound states of molecules such as Cs_2 . The method is based on solving a set of coupled differential equations by propagation, without relying on a basis set for the interatomic coordinate. This is much more efficient than using a radial basis set and allows the use of much larger basis sets of spin functions. It also eliminates problems with calculating bound states very near to dissociation, because the propagation can be extended to very large separations at very little expense. The new method makes it possible for the first time to

carry out fully converged calculations on bound states of Cs_2 , including anisotropic couplings due to spin-spin and second-order spin-orbit interactions, and to characterize avoided crossings between pairs of levels.

We have compared the results of converged calculations using the current best Cs_2 model potentials with experimental measurements on the near-dissociation states of Cs_2 in a magnetic field. The model generally performs well for s , d and g states (with $L = 0, 2$ and 4), though even there there are quantitative discrepancies of up to 0.05 mT in the magnetic fields at which levels cross. The discrepancies are much larger (0.5 mT) for l states ($L = 8$). The strengths of the avoided crossings also appear to be systematically underestimated by the current model. These discrepancies should in future allow the development of improved models for the potential curves and couplings in the Cs_2 dimer. Such model improvement is both desirable and possible, not only for near-threshold levels but also to provide an improved representation of more deeply bound states such as those measured by Vanhaecke *et al.* [6]. High-quality models are also important for proposals to use precision measurements on Cs_2 for fundamental physics studies [35, 36].

VI. ACKNOWLEDGEMENTS

P.S. Julianne acknowledges the Office of Naval Research for partial support. J. M. Hutson is grateful to EPSRC for support under the ESF EUROCORES Programme EuroQUAM.

APPENDIX A: MATRIX ELEMENTS

In the decoupled basis set (5), the matrix elements of the isotropic potential operator $\hat{V}^c(R)$ between primitive (unsymmetrized) basis functions are

$$\langle s_1 m_{s_1} i_1 m_{i_1} s_2 m_{s_2} i_2 m_{i_2} L M_L | \hat{V}^c(R) | s_1 m'_{s_1} i_1 m'_{i_1} s_2 m'_{s_2} i_2 m'_{i_2} L' M'_L \rangle = \delta_{LL'} \delta_{M_L M'_L} \delta_{m_{i_1} m'_{i_1}} \delta_{m_{i_2} m'_{i_2}} \sum_S V_S(R) (-1)^{2s_1 - 2s_2 + m_{s_1} + m_{s_2} + m'_{s_1} + m'_{s_2}} (2S + 1) \begin{pmatrix} s_1 & s_2 & S \\ m_{s_1} & m_{s_2} & -m_{s_1} - m_{s_2} \end{pmatrix} \begin{pmatrix} s_1 & s_2 & S \\ m'_{s_1} & m'_{s_2} & -m'_{s_1} - m'_{s_2} \end{pmatrix}. \quad (\text{A1})$$

The corresponding matrix elements of the spin-spin operator are

$$\langle s_1 m_{s_1} i_1 m_{i_1} s_2 m_{s_2} i_2 m_{i_2} L M_L | \hat{V}^d(R) | s_1 m'_{s_1} i_1 m'_{i_1} s_2 m'_{s_2} i_2 m'_{i_2} L' M'_L \rangle = \delta_{m_{i_1} m'_{i_1}} \delta_{m_{i_2} m'_{i_2}} \lambda(R) (-1)^{s_1 + s_2 - m_{s_1} - m_{s_2} - M_L} [s_1(s_1 + 1)(2s_1 + 1)s_2(s_2 + 1)(2s_2 + 1)(2L + 1)(2L' + 1)]^{1/2} \begin{pmatrix} L & 2 & L' \\ 0 & 0 & 0 \end{pmatrix} \sum_{q_1 q_2} \begin{pmatrix} L & 2 & L' \\ -M_L & -q_1 - q_2 & M'_L \end{pmatrix} \begin{pmatrix} 1 & 1 & 2 \\ q_1 & q_2 & -q_1 - q_2 \end{pmatrix} \begin{pmatrix} s_1 & 1 & s_1 \\ -m_{s_1} & q_1 & m'_{s_1} \end{pmatrix} \begin{pmatrix} s_2 & 1 & s_2 \\ -m_{s_2} & q_2 & m'_{s_2} \end{pmatrix}, \quad (\text{A2})$$

where for any individual matrix element the sums over q_1 and q_2 collapse because of the selection rules imposed by the last two 3- j symbols. The matrix elements of the atomic nuclear spin operators are particularly simple in this basis set,

$$\langle s_1 m_{s_1} i_1 m_{i_1} s_2 m_{s_2} i_2 m_{i_2} L M_L | \hat{i}_1 \cdot \hat{s}_1 | s_1 m'_{s_1} i_1 m'_{i_1} s_2 m'_{s_2} i_2 m'_{i_2} L' M'_L \rangle = \delta_{LL'} \delta_{m_{s_2} m'_{s_2}} \delta_{m_{i_2} m'_{i_2}} \langle s_1 m_{s_1} i_1 m_{i_1} | \hat{i}_1 \cdot \hat{s}_1 | s_1 m'_{s_1} i_1 m'_{i_1} \rangle \quad (\text{A3})$$

where

$$\langle s_1 m_{s_1} i_1 m_{i_1} | \hat{i}_1 \cdot \hat{s}_1 | s_1 m_{s_1} i_1 m_{i_1} \rangle = m_{i_1} m_{s_1}; \quad (\text{A4})$$

$$\langle s_1 m_{s_1} i_1 m_{i_1} | \hat{i}_1 \cdot \hat{s}_1 | s_1 m_{s_1} \pm 1 i_1 m_{i_1} \mp 1 \rangle = [s_1(s_1 + 1) - m_{s_1}(m_{s_1} \pm 1)]^{1/2} [i_1(i_1 + 1) - m_{i_1}(m_{i_1} \mp 1)]^{1/2}, \quad (\text{A5})$$

and similarly for $\hat{i}_2 \cdot \hat{s}_2$. The matrix elements of \hat{L}^2 are simply

$$\begin{aligned} \langle s_1 m_{s_1} i_1 m_{i_1} s_2 m_{s_2} i_2 m_{i_2} L M_L | \hat{L}^2 | s_1 m'_{s_1} i_1 m'_{i_1} s_2 m'_{s_2} i_2 m'_{i_2} L' M'_L \rangle = \\ \delta_{LL'} \delta_{M_L M'_L} \delta_{m_{s_1} m'_{s_1}} \delta_{m_{i_1} m'_{i_1}} \delta_{m_{s_2} m'_{s_2}} \delta_{m_{i_2} m'_{i_2}} L(L + 1), \end{aligned} \quad (\text{A6})$$

and those of the Zeeman operator are

$$\begin{aligned} \langle s_1 m_{s_1} i_1 m_{i_1} s_2 m_{s_2} i_2 m_{i_2} L M_L | \hat{g}_e \mu_B B \hat{s}_{zj} + g_n \mu_B B \hat{i}_{zj} | s_1 m'_{s_1} i_1 m'_{i_1} s_2 m'_{s_2} i_2 m'_{i_2} L' M'_L \rangle = \\ \delta_{LL'} \delta_{M_L M'_L} \delta_{m_{s_1} m'_{s_1}} \delta_{m_{i_1} m'_{i_1}} \delta_{m_{s_2} m'_{s_2}} \delta_{m_{i_2} m'_{i_2}} (g_e \mu_B B \hat{m}_{s_j} + g_n \mu_B B m_{i_j}). \end{aligned} \quad (\text{A7})$$

All the calculations in the present paper used basis functions symmetrized for exchange of two identical particles with $s_1 = s_2 = s$ and $i_1 = i_2 = i$. For $m_{s_1} = m_{s_2}$ or $m_{i_1} = m_{i_2}$ the symmetrized functions are identical to the unsymmetrized ones, except that only even L is allowed for bosons and only odd L for fermions. For $m_{s_1} \neq m_{s_2}$ or $m_{i_1} \neq m_{i_2}$, the symmetrized functions are

$$[|s m_{s_1} i m_{i_1} s m_{s_2} i m_{i_2} L M_L \rangle \pm (-1)^L |s m_{s_2} i m_{i_2} s m_{s_1} i m_{i_1} L M_L \rangle] / \sqrt{2}, \quad (\text{A8})$$

with the + sign for bosons and the – sign for fermions.

The Hamiltonian in the basis set, Eq. (4), used in the DVR calculations can be derived from the Hamiltonian in the uncoupled basis by performing a unitary transformation, namely, the transformation $|\alpha_j m_{fj}\rangle$ to $|s_j m_{sj}\rangle |i_j m_{ij}\rangle$ for each of the two atoms ($j=1$ or 2). The transformation depends on the magnetic field strength [37]. In practice, the eigenvectors for the monomer h_j must be evaluated. As m_{fj} is conserved at most a 2×2 matrix needs to be diagonalized. Bose/Fermi symmetrization is ensured by

$$[|\alpha_1 m_{f1} \alpha_2 m_{f2}, L M_L \rangle \pm (-1)^L |\alpha_2 m_{f2} \alpha_1 m_{f1}, L M_L \rangle] / \sqrt{2}$$

when $\alpha_1 \neq \alpha_2$ or $m_{f1} \neq m_{f2}$. The state with $\alpha_1 = \alpha_2$ and $m_{f1} = m_{f2}$ exists only for even (odd) L for bosonic (fermionic) atoms respectively.

-
- [1] T. Weber, J. Herbig, M. Mark, H.-C. Nägerl, and R. Grimm, *Science* **299**, 232 (2003).
 - [2] J. Herbig, T. Kraemer, M. Mark, T. Weber, C. Chin, H.-C. Nägerl, and R. Grimm, *Science* **301**, 1510 (2003).
 - [3] T. Kraemer, M. Mark, P. Waldburger, J. G. Danzl, C. Chin, B. Engeser, A. D. Lange, K. Pilch, A. Jaakkola, H.-C. Nägerl, et al., *Nature* **440**, 315 (2006).
 - [4] K. Szymaniec, W. Chalupczak, E. Tiesinga, C. J. Williams, S. Weyers, and R. Wynands, *Phys. Rev. Lett.* **98**, 153002 (2007).
 - [5] R. A. Hart, X. Xu, R. Legere, and K. Gibble, *Nature* **446**, 892 (2007).
 - [6] N. Vanhaecke, C. Lisdat, B. Tjampens, D. Comparat, A. Crubellier, and P. Pillet, *Eur. Phys. J. D* **28**, 351 (2004).
 - [7] M. Mark, T. Kraemer, P. Waldburger, J. Herbig, C. Chin, H.-C. Nägerl, and R. Grimm, *Phys. Rev. Lett.* **99**, 113201 (2007).
 - [8] M. Mark, F. Ferlaino, S. Knoop, J. G. Danzl, T. Kraemer, C. Chin, H.-C. Nägerl, and R. Grimm, *Phys. Rev. A* **76**, 042514 (2007).
 - [9] C. Chin, V. Vuletić, A. J. Kerman, and Chu, *Phys. Rev. Lett.* **85**, 2717 (2000).
 - [10] P. J. Leo, C. J. Williams, and P. S. Julienne, *Phys. Rev. Lett.* **85**, 2721 (2000).
 - [11] C. Chin, A. J. Kerman, V. Vuletić, and S. Chu, *Phys. Rev. Lett.* **90**, 033201 (2003).
 - [12] C. Chin, V. Vuletić, A. J. Kerman, S. Chu, E. Tiesinga, P. J. Leo, and C. J. Williams, *Phys. Rev. A* **70**, 032701 (2004).
 - [13] M. D. Lee, T. Köhler, and P. S. Julienne, *Phys. Rev. A* **76**, 012720 (2007).
 - [14] J. M. Hutson, *Comput. Phys. Commun.* **84**, 1 (1994).
 - [15] T. Köhler, K. Góral, and P. S. Julienne, *Rev. Mod. Phys.* **78**, 1311 (2006).
 - [16] F. Lang, P. van der Straten, B. Brandstätter, G. Thalhammer, K. Winkler, P. S. Julienne, R. Grimm, and J. Hecker Denschlag, *Nature Phys.* **4**, 223 (2008).
 - [17] H. T. C. Stoof, J. M. V. A. Koelman, and B. J. Verhaar, *Phys. Rev. B* **38**, 4688 (1988).
 - [18] D. T. Colbert and W. H. Miller, *J. Comp. Phys.* **96**, 1982 (1992).

- [19] E. Tiesinga, C. J. Williams, and P. S. Julienne, Phys. Rev. A **57**, 4257 (1998).
- [20] E. Anderson, Z. Bai, C. Bischof, J. W. Demmel, J. J. Dongarra, J. Du Croz, A. Greenbaum, S. Hammarling, A. McKenney, S. Ostrouchov, et al., *LAPACK User's Guide* (SIAM, Philadelphia, 1992).
- [21] The scattering resonance positions given in Ref. [12] were calculated by a propagator method, and are not subject to the basis set restrictions that apply to bound states.
- [22] B. R. Johnson, J. Chem. Phys. **69**, 4678 (1978).
- [23] J. M. Hutson, *Bound computer program, version 5*, distributed by Collaborative Computational Project No. 6 of the UK Engineering and Physical Sciences Research Council (1993).
- [24] M. H. Alexander and D. E. Manolopoulos, J. Comp. Phys. **86**, 2044 (1987).
- [25] M. Krauss and W. J. Stevens, J. Comp. Phys. **93**, 4236 (1990).
- [26] A. J. Moerdijk, B. J. Verhaar, and A. Axelsson, Phys. Rev. A **51**, 4852 (1995).
- [27] F. H. Mies, C. J. Williams, P. S. Julienne, and M. Krauss, J. Res. Natl. Inst. Stand. Technol **101**, 521 (1996).
- [28] P. J. Leo, E. Tiesinga, P. S. Julienne, and D. K. Walker, Phys. Rev. Lett. **81**, 1389 (1998).
- [29] S. Kotochigova, E. Tiesinga, and P. S. Julienne, Phys. Rev. A **63**, 012517 (2001).
- [30] F. Ferlaino, S. Knoop, M. Berninger, M. Mark, H.-C. Nägerl, and R. Grimm, *private communication* (2008).
- [31] P. S. Julienne, E. Tiesinga, and T. Köhler, J. Mod. Optics **51**, 1787 (2004).
- [32] A. D. Lange, K. Pilch, A. Prantner, F. Ferlaino, B. Engeser, H. C. Nägerl, R. Grimm, and C. Chin, arXiv p. in preparation (2008).
- [33] F. Ferlaino and R. Grimm, *private communication* (2008).
- [34] S. T. Thompson, E. Hodby, and C. E. Wieman, Phys. Rev. Lett. **95**, 190404 (2005).
- [35] C. Chin and V. V. Flambaum, Phys. Rev. Lett. **96**, 230801 (2006).
- [36] D. DeMille, S. Sainis, J. Sage, T. Bergeman, S. Kotochigova, and E. Tiesinga, Phys. Rev. Lett. **100**, 043202 (2008).
- [37] G. Breit and I. I. Rabi, Phys. Rev. A **38**, 2082 (1931).